Electronic Supplementary Material (ESI) for ChemComm.

Supporting Information

Exploiting Halido ligands to control nucleation pathways and Pt···Pt interactions in supramolecular co-polymerizations

Jonas Matern,[a] Zulema Fernández,[a] and Gustavo Fernández*[a]

[a] *Organisch-Chemisches Institut, Westfälische Wilhelms-Universität Münster, Corrensstraße 36, 48149 Münster, Germany. E-mail: fernandg@uni-muenster.de*

Table of Contents

Supplementary Experiments/Figures

Preliminary Self-Assembly Studies

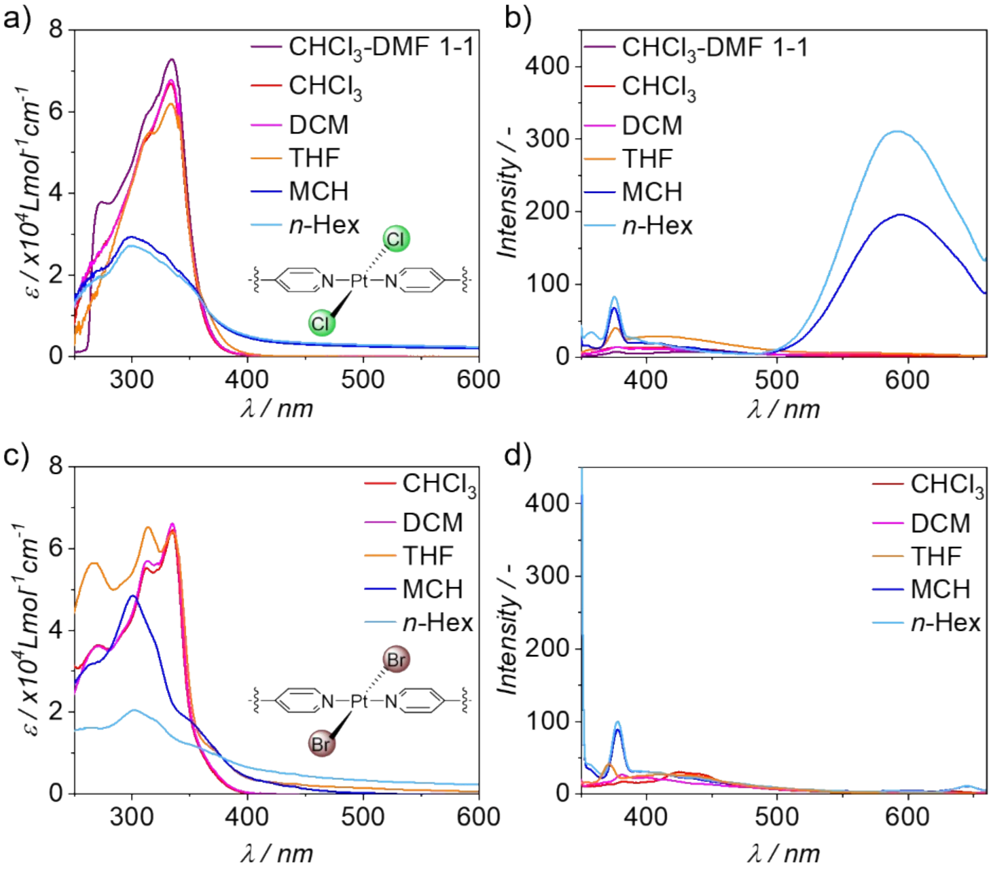

Figure S1. UV/vis absorption (left panel) and emission spectra (right panel), of **1** (a, b) and **2** (c,d) in different solvents (c = 20 µM, T = 298 K, λ_{ex} = 333 nm for **1**; λ_{ex} = 335 nm for **2**). All emission spectra were measured at the same detector sensitivity and the y-axes were scaled to the same intensity for a better comparison.

The solvent-dependent absorption spectra indicate a similar self-assembly behavior for the two complexes: The compounds are molecularly dissolved in good solvents, such as $CHCl_3$, THF and DCM, with ^{1}MLCT absorption maxima at λ_{max} = 333 nm (**1**) and λ_{max} = 335 nm (**2**) and a should band/second maximum at ~314 nm (metal-perturbed ^{1}IL), for **1** and **2**, respectively. In apolar *n*-hexane (*n*-Hex) and methylcyclohexane (MCH), the absorbance is strongly diminished and blue-shifted to around 300 nm for both complexes, accompanied by a Tyndall effect at longer wavelengths, indicating the formation of elongated supramolecular polymers (SPs). Precipitation occurs for **2** in *n*-Hex over time, as evident from the significant scattering and drop in absorbance (Figure S1c).

The emission spectra on the other hand exhibit drastic differences: Despite the similar aggregation tendency witnessed in the absorption studies, the emission spectra of **2** lack any signs of the low-energy ^{3}MMLCT emission band at ~600 nm. However, the low intensity ligand centered emission between 375-500 nm is similar to the one of **1**. These observations indicate that **2** cannot develop Pt···Pt interactions in the aggregates, presumably due to the higher steric demand of the bromido ligands.

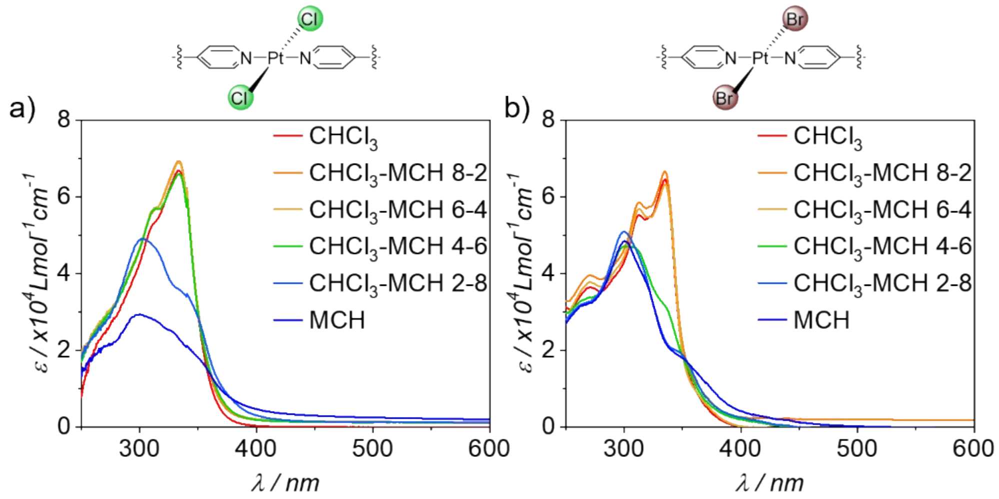

Figure S2. UV/vis absorption spectra of complexes **1** (a) and **2** (b) in solvent mixtures of different $CHCl_3$/MCH ratios (*c* = 20 µM, *T* = 298 K).

In the case of **1**, the complex is molecularly dissolved under ambient conditions in solutions containing $CHCl_3$ volume fractions exceeding 30 % *v/v*, whereas the aggregates precipitate at $CHCl_3$ contents lower than 20 % *v/v*. Due to a stronger aggregation tendency as a result of increased solvophobic forces in the bromido complex **2**,[1] the self-assembled structures can tolerate an increase of approx. ~10 % *v/v* $CHCl_3$ in comparison to **1**. Hence, the self-assembly of the complexes in solution was studied in mixtures of MCH with 20-30 % *v/v* $CHCl_3$.

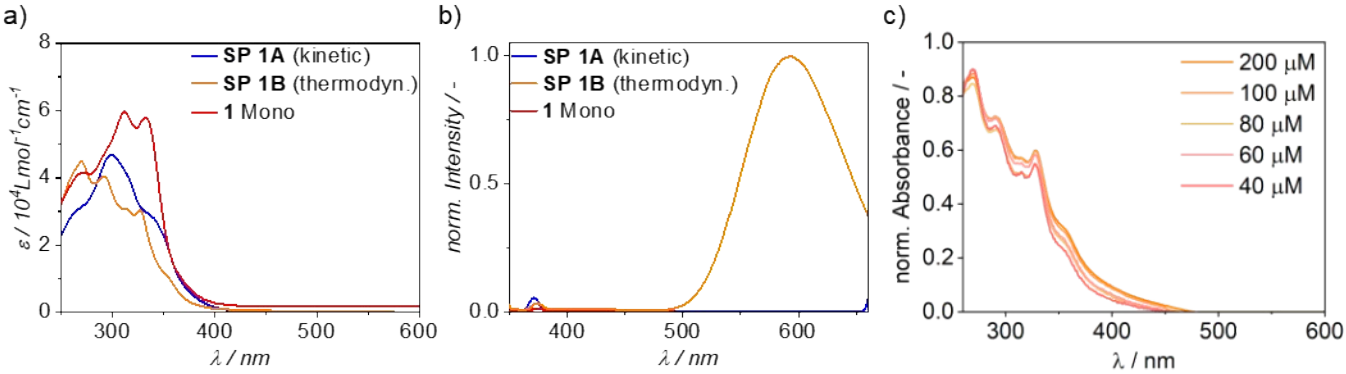

Figure S3. UV/vis absorption (a) and emission spectra (b) of monomer (red), kinetic (blue) and thermodynamic aggregate (orange) of **1** (MCH/$CHCl_3$ 8:2, *c* = 20 µM, *T* = 298 K). c) Normalized UV/Vis absorption spectra for the thermodynamic aggregate (**SP 1B**) at different concentrations (MCH/$CHCl_3$ 8:2, *T* = 298 K).

All three species can be obtained in the same solvent mixture (MCH/$CHCl_3$ 8:2). The monomer is present at high temperatures, the kinetic aggregate is formed upon cooling with fast rates (5 Kmin^{-1})/without stirring, whereas the thermodynamic aggregate is obtained upon cooling at a rate of 1 Kmin^{-1} while stirring the solution during the cooling process. For **1B** at low concentrations, the lack of a clearly noticeable ^{1}MMLCT band in UV/Vis (see Fig. S3a) indicates weak ground-state metal-metal interactions. As observed in Fig. 3b, metal-metal interactions are stronger in the excited state than in the ground state and we assigned this featureless emission at ca. 600 nm to ^{3}MMLCT with excimeric character. Concentration-dependent UV/Vis experiments of **1B** under thermodynamic conditions revealed that the shoulder band at ca. 355 nm becomes more pronounced upon increasing concentration and induces a tailing that reaches up to 450-475 nm. These results seem to indicate stronger ground-state Pt-Pt interactions at higher concentrations.

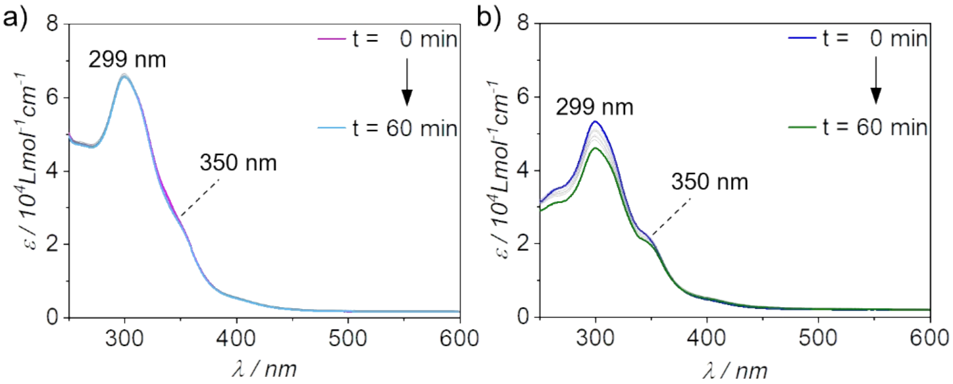

Figure S4. Time-dependent UV/vis absorption spectra of a solution of **2** after different preparation protocols under kinetic control (MCH/$CHCl_3$ 7:3, c = 20 µM, T = 298 K). a) Thermal quenching (instant cooling of a hot monomer solution from 95 °C to 0°C). b) Addition of an excess of MCH to a solution of monomers in $CHCl_3$ (solvophobic quenching).

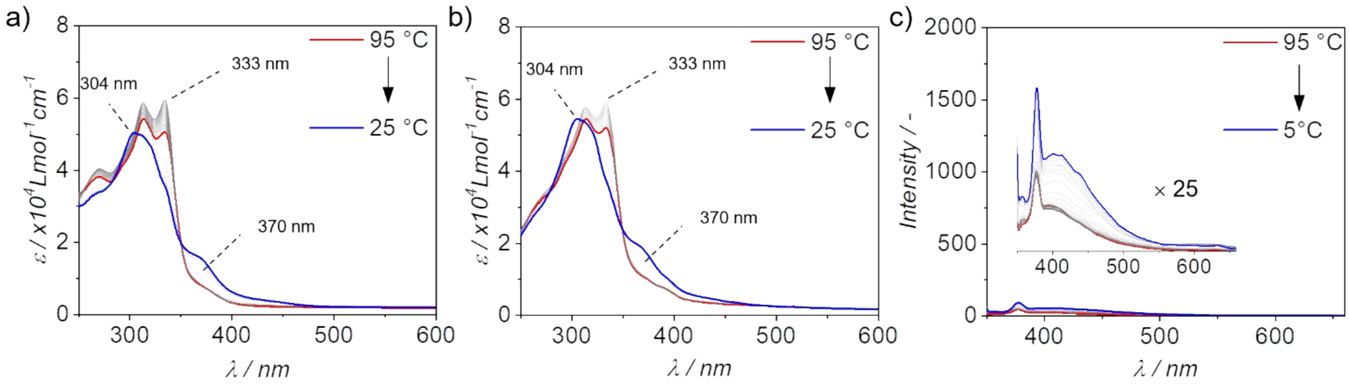

Figure S5. a,b) VT-UV/vis absorption spectra upon cooling a solution of **2** at 1 Kmin^{-1} without (a) and with stirring (b). c) Corresponding emission spectra (c = 20 µM, MCH/$CHCl_3$ 7:3).

In the case of complex **2**, cooling at 1 Kmin^{-1} yields only a single type of one poorly emissive aggregated species (λ^{em}_{max} ~ 400 nm), regardless if the solution is stirred or not.

Morphology Studies of 2

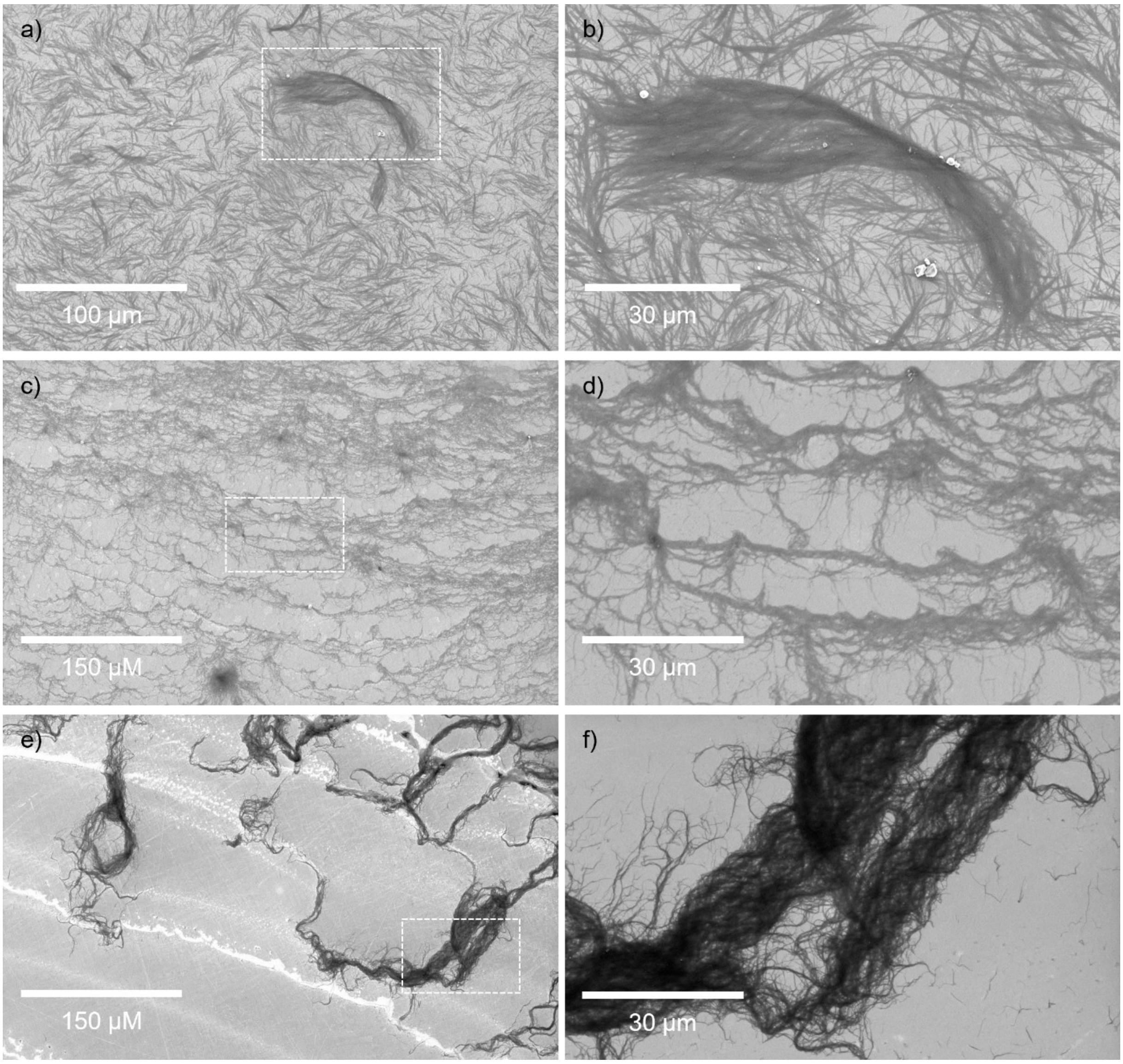

Figure S6. SEM images of the SPs of **2** formed under kinetic conditions (a+b, **B**-type SPs) and thermodynamic conditions (c-f, **A**-type SPs). Solution conditions before drop-casting: c = 20 µM, MCH-$CHCl_3$ 7-3.

The images depicted in (e) & (f) were obtained after ageing the solution that was used for images (c) & (d). Thus, upon ageing, the A-type SPs form bundled SP clusters. In corresponding UV/vis absorption spectra, this bundling only led to slight changes in the intensity/sharpness of the absorption, however, without a shift of the absorption maxima.

Comparison of the SPs of 1 & 2

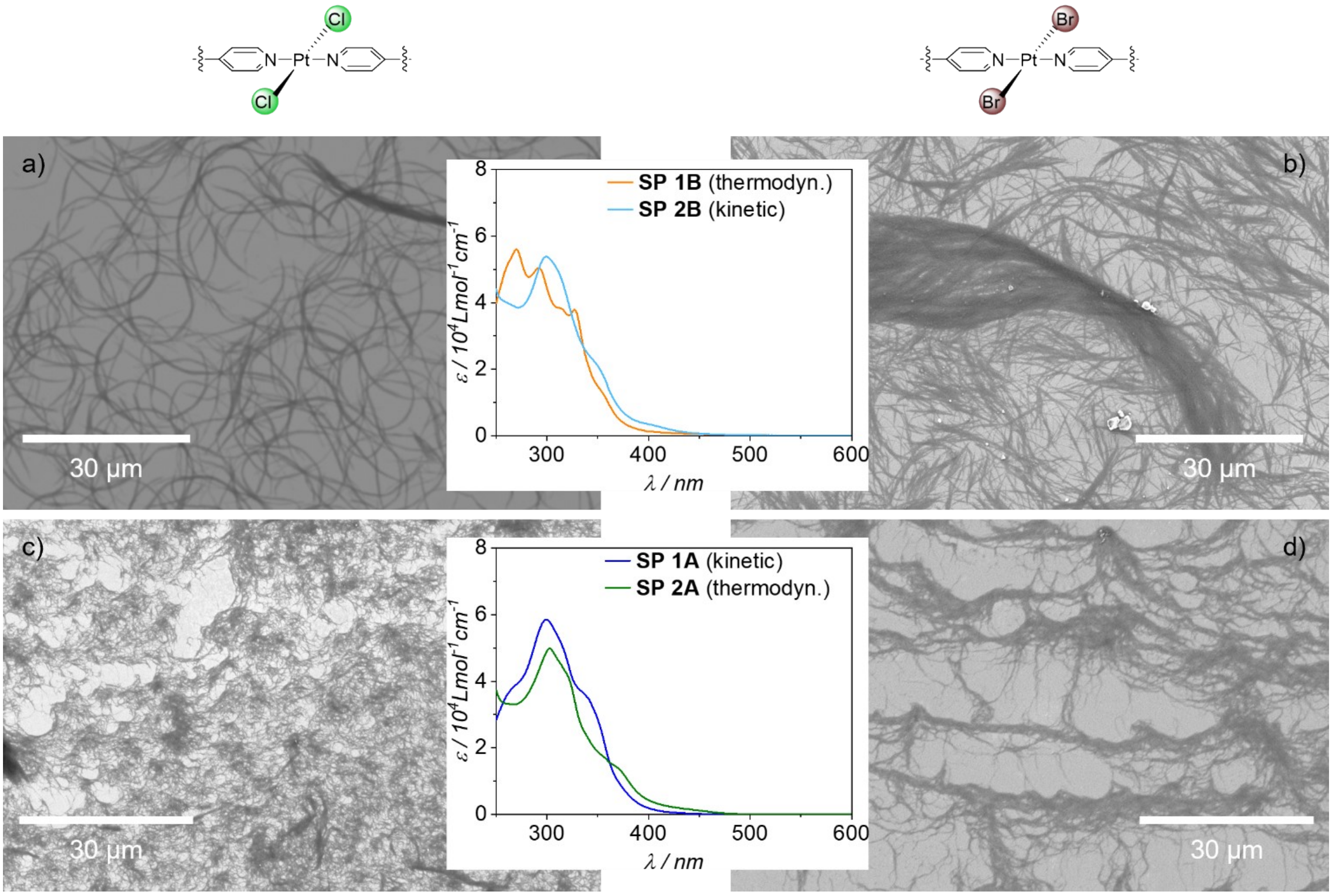

Figure S7. Comparison of the morphologies (SEM) of the **B**-type (a+b) and **A**-type SPs (c+d) of **1** (left panel) and **2** (right panel). The central insets show the absorption spectra of the respective solutions used to prepare the samples for SEM imaging (*c* = 20 µM).

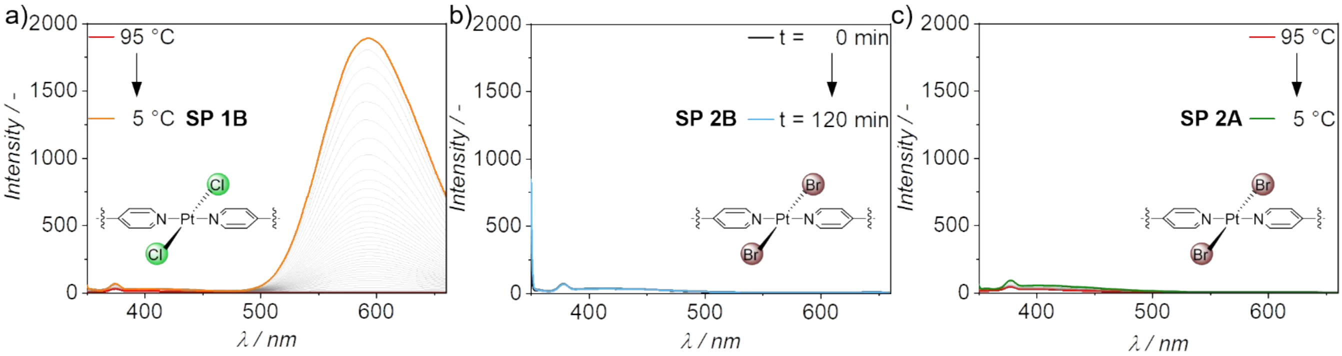

Figure S8. Comparison of the emission spectra upon formation of **SP 1B** (a, cooling @ 1 Kmin^{-1}, stirring @ 800 rpm) with those during the formation of **SP 2B** (b, solvophobic quenching) and **SP 2A** (c, cooling @ 1 Kmin^{-1}, stirring @ 800 rpm, in all cases *c* = 20 µM). For a better comparison, the y-axes were scaled equally in all three plots.

Thermodynamic Stability Studies

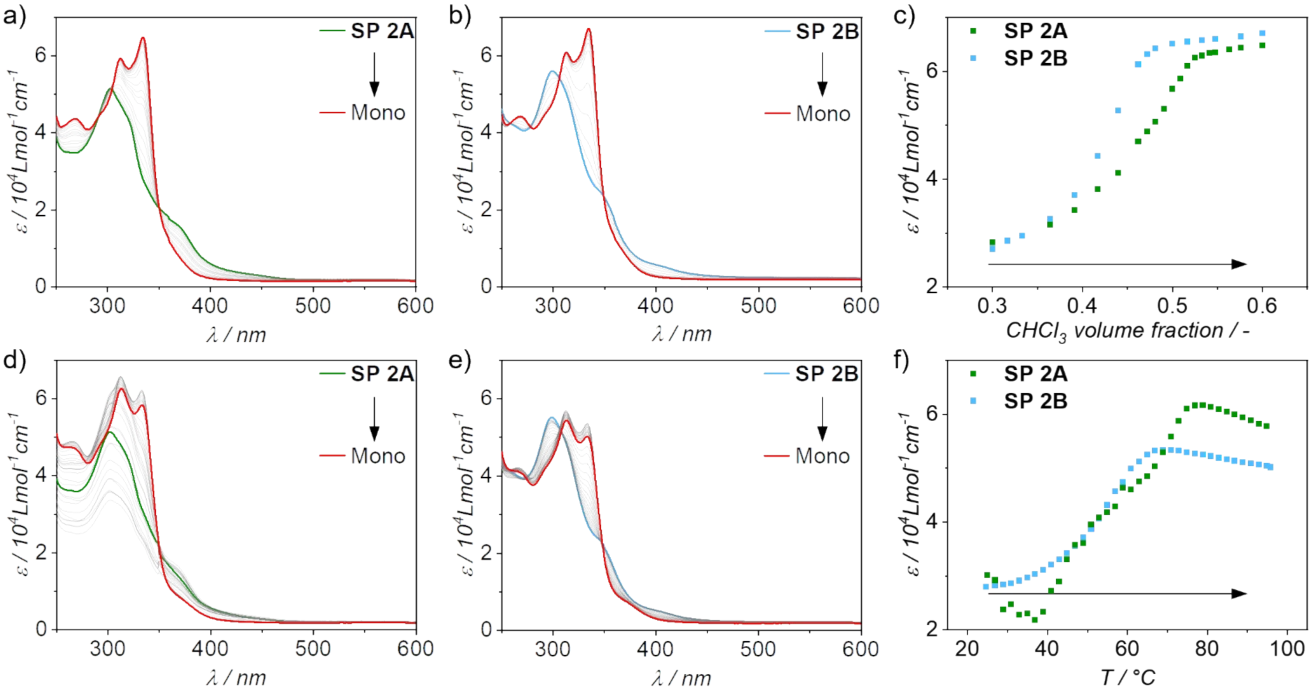

Figure S9: Comparison of the disassembly of **2A** and **2B** in denaturation (a-c) and heating studies (d-f). a-c) UV/vis spectra during the denaturation of **2A** (a) and **2B** (b) with $CHCl_3$ and corresponding plot of the absorbance at 335 nm against the $CHCl_3$ volume fraction (c). d-f) UV/vis spectra during the heating of **2A** (d) and **2B** (e) and corresponding plot of the absorbance at 335 nm against the temperature (f).

In both cases, disassembly of **2B** occurs prior to the disassembly of **2A**, revealing the higher stability of **2A** (→ **2A** is the thermodynamic SP, **2B** the kinetic one).

Packing Mode Analysis

The packing modes in the SPs by FTIR and ^{1}H NMR. The thin film ATR-FTIR spectra of **2A** and **2B** are practically identical, indicating classical amide-to-amide hydrogen bonds (H-bonds) in both SPs (see Fig. S10 below).

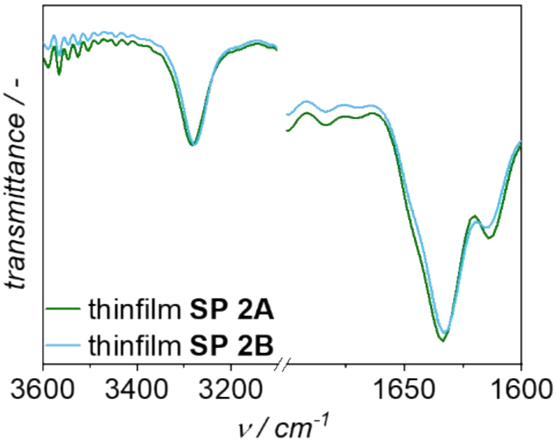

Figure S10. ATR-FTIR spectra of thin films obtained from solutions of **2A** (green) and **2B** (cyan).

In both cases, the N-H and C=O stretching frequencies are practically the same ($\nu_{N\text{-}H}$ = 3282 cm^{-1} (**2A**), 3278 cm^{-1} (**2B**); $\nu_{C=O}$ = 1633 cm^{-1} for both). This could be due the fact that either the strength of the intermolecular amide-to-amide H-bonding is very similar in the two SP species, or that upon drying, kinetic **2B** is converted into **2A**, due to the higher stability of the latter.

VT-^{1}H NMR studies allowed us to monitor the self-assembly of **2A**, whereas formation of **2B** was monitored by solvent-dependent NMR in $CDCl_3$/MCH-d_{14} (Fig. S11 & S12). In both cases, the typical features of intermolecular H-bonding are observed, i.e. strong deshielding of the amide protons. In close resemblance to **1B**, the pyridine α-protons are deshielding upon formation of **2B**, indicating sterically unfavourable interactions of these protons with the bromido ligands upon coplanarization of the pyridine with respect to the PtL_4 plane (for comparison of **1** and **2** see Fig. S13). In contrast to **1B**, none of the other aromatic protons is shielding, demonstrating the absence of aromatic interactions. The self-assembly of **2A** on the other hand, is accompanied by slight upfield shifts of the pyridine protons and the protons of the central phenyl ring, suggesting some degree of aromatic interactions.

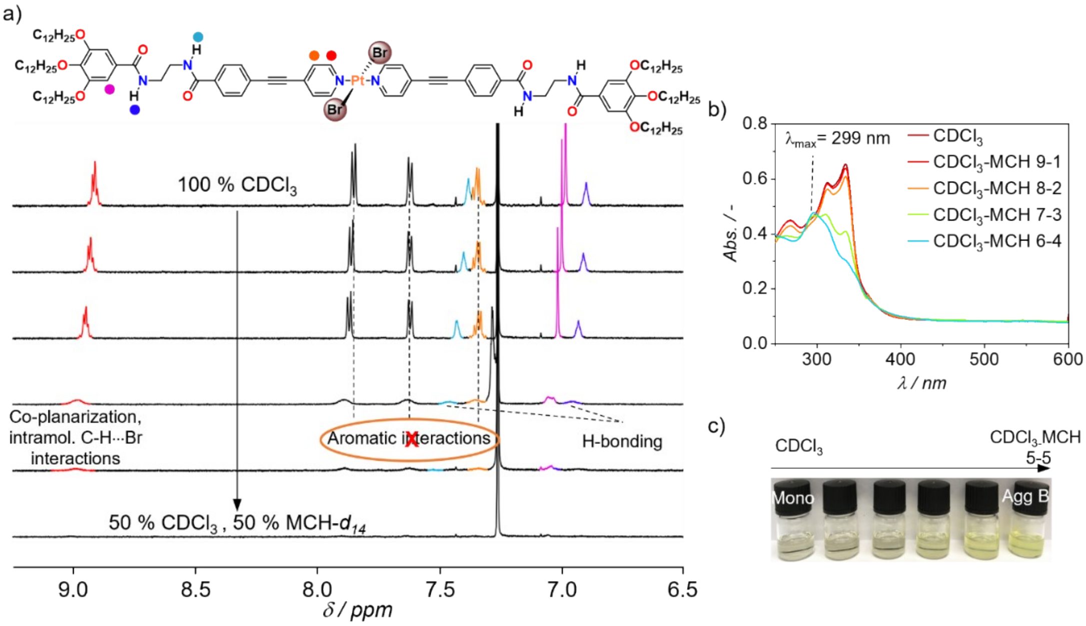

Figure S11. Packing mode studies of **2** upon decreasing the solvent polarity of the solution from pure $CDCl_3$ by stepwise addition of MCH-d_{14}, inducing self-assembly into **SP 2B** (c = 1 mM, T = 298 K). a) ^{1}H NMR spectra and chemical structure illustrating the assignments of the resonances. b) Corresponding UV/vis spectra recorded of the solutions prior to the NMR experiment. c) Photographs of the solutions.

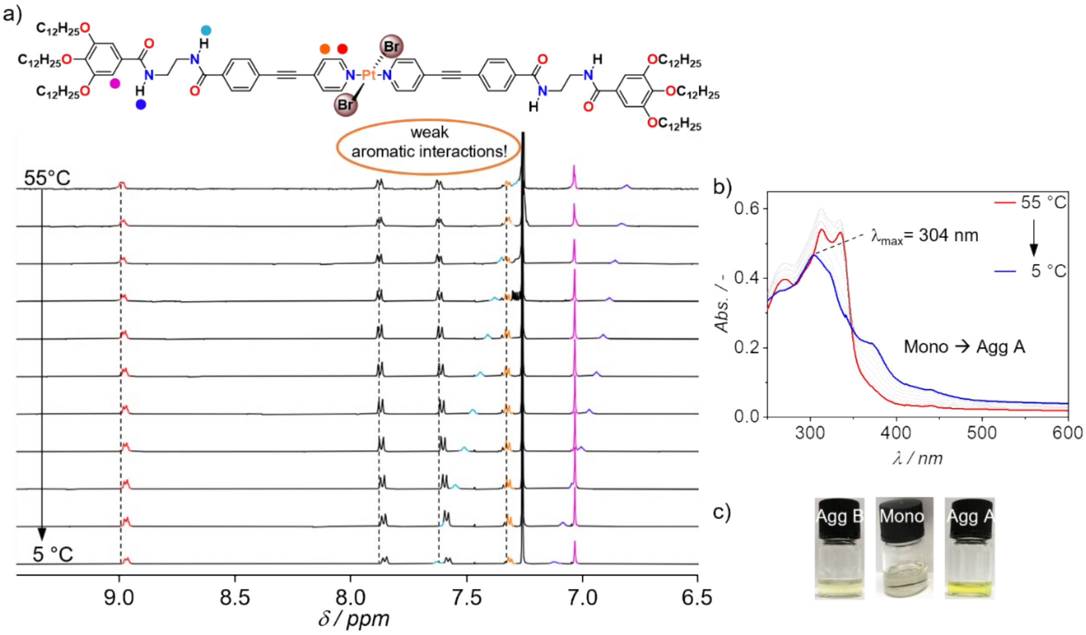

Figure S12. Packing mode studies of **2** upon cooling a hot monomer solution at a rate of 1 Kmin^{-1}, inducing self-assembly into **SP 2A** (c = 1 mM, MCH-d_{14}/$CDCl_3$ 3:7). a) ^{1}H NMR spectra and chemical structure illustrating the assignments of the resonances. b) Corresponding UV/vis spectra recorded under equal conditions. c) Photographs comparing the solutions of **2B**, monomers and **2A**.

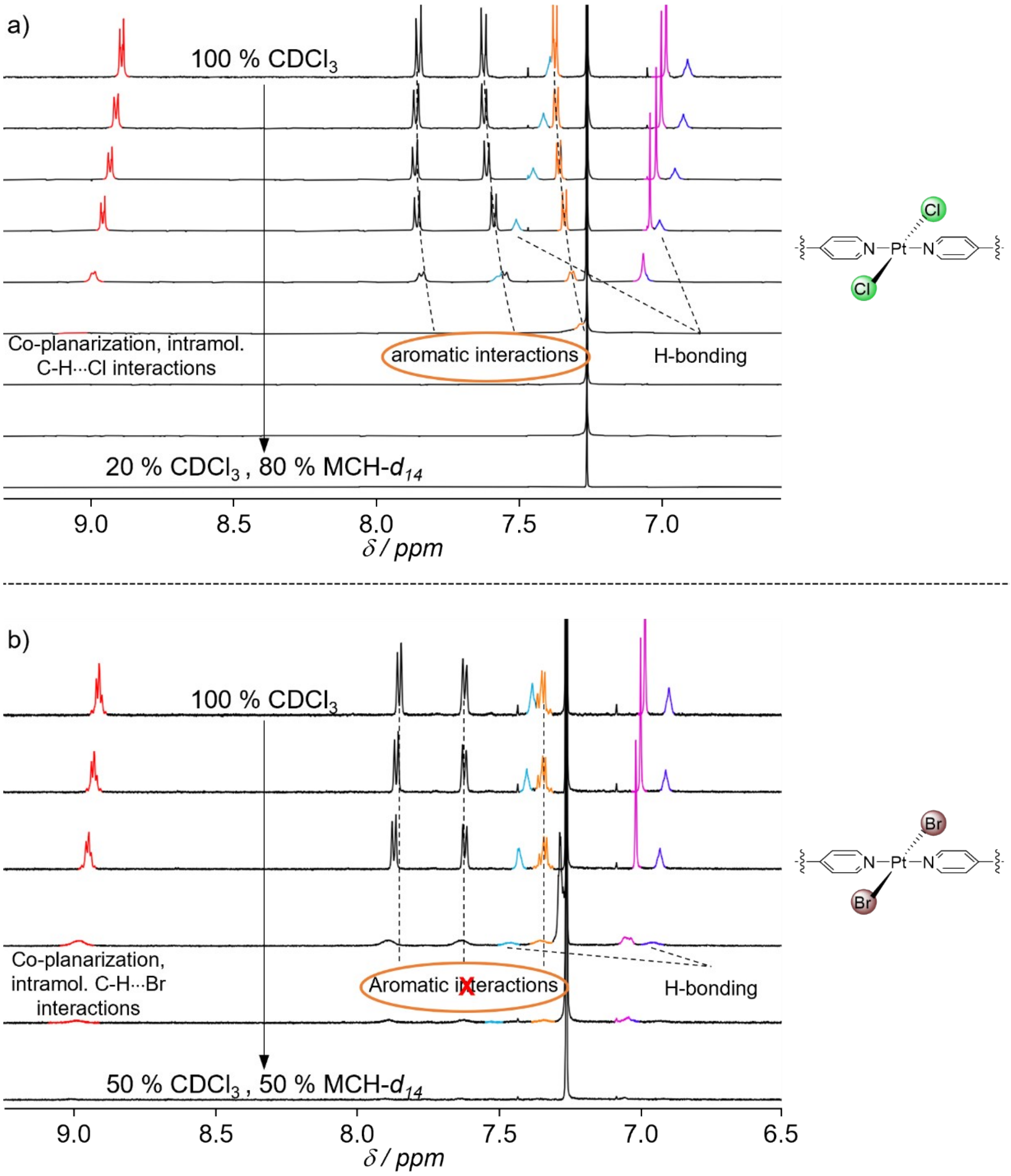

Figure S13. Comparison of the ^{1}H NMR spectra during the self-assembly of **1B** (a) and **2B** (b) upon decreasing the solvent polarity of the solution from pure $CDCl_3$ by addition of MCH-d_{14} (c = 1 mM, T = 298 K).

While in both cases the deshielding of the resonance of the α-pyridine protons (red) indicates repulsive interactions between these protons and the halogenido ligands upon coplanarization, the resonances of the β-pyridine proton (orange) and the protons of the central phenyl-unit (black) behave differently: In the case of **1B**, these protons are shielding as a result of aromatic interactions, whereas for **2B**, they are practically unaffected, indicating no/very weak aromatic interactions. The resonances of the amide protons (cyan & blue) and the aromatic proton of the phenyl ring bearing the solubilizing chains (pink) on the other hand exhibit the same downfield shifts upon self-assembly, diagnostic of amide-to-amide H-bonding.

Thermal Copolymerization Experiments

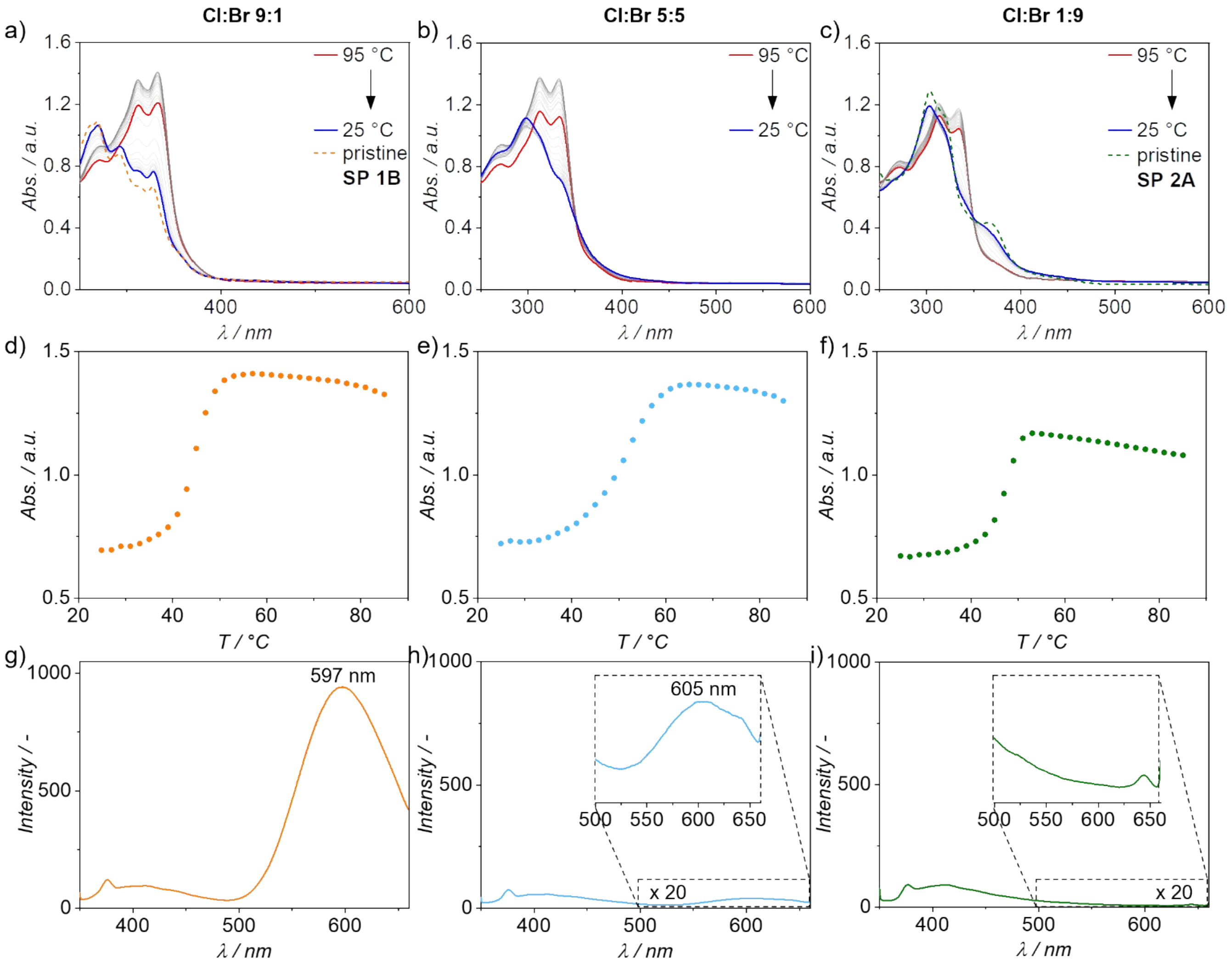

Figure S14. Co-assembly experiments at different **1**:**2** ratios. a-c) VT-UV/vis spectra upon cooling the mixtures at a rate of 1 Kmin^{-1}, while stirring at 800 rpm (→ thermodynamic control, c_{tot} = 20 µM, MCH/$CHCl_3$ 7:3). d-f) Corresponding one-step cooling curves extracted from the VT-UV/vis spectra at λ = 333 nm. g-i) Emission spectra of the solutions, recorded subsequent to the VT-UV/vis experiments.

Seed-mediated/Living Supramolecular Copolymerization

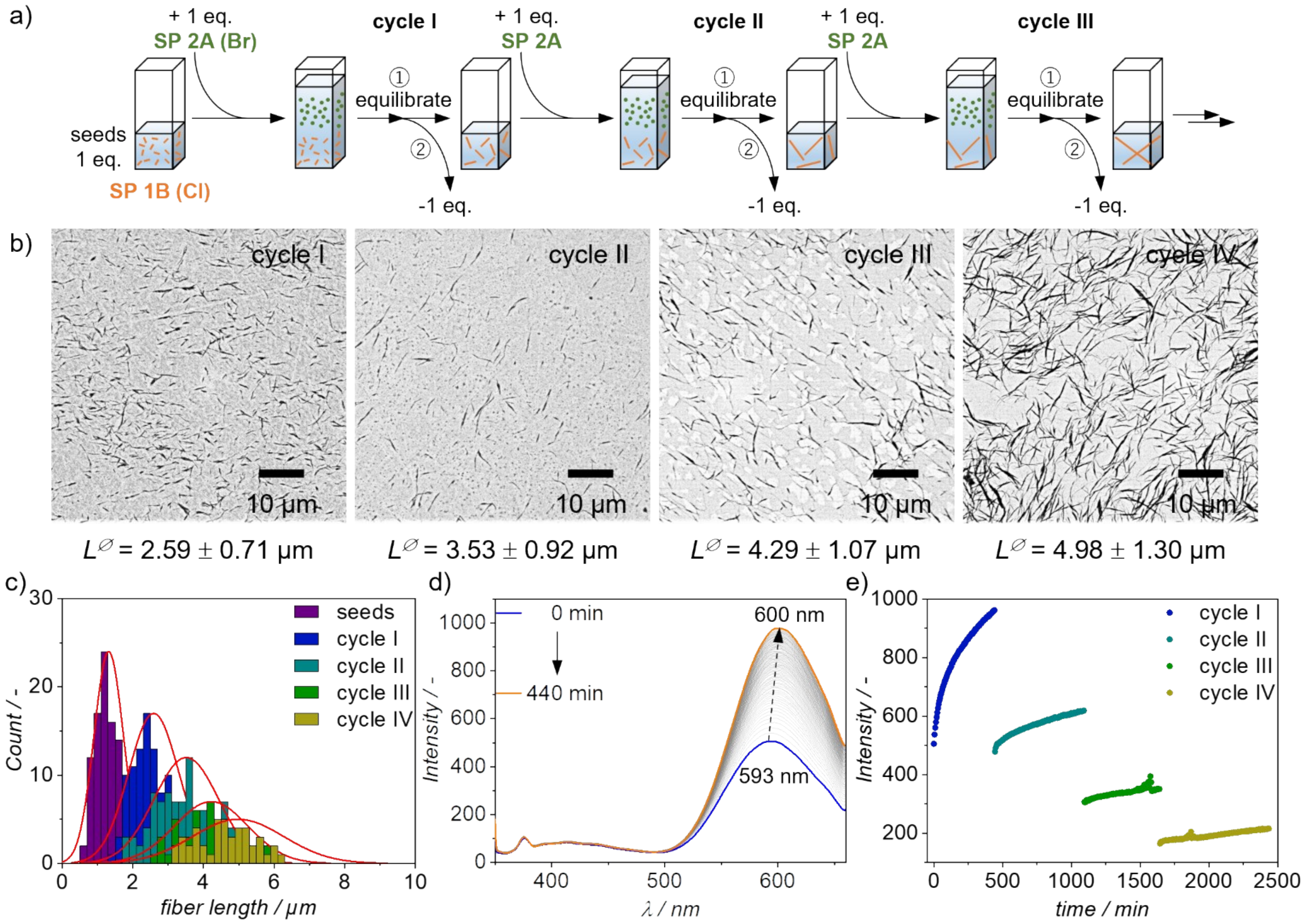

Figure S15. Seed-mediated co-LSP using **1B** seeds and **2A** feedstock (experiment (1)). a) Schematic representation of the experimental procedure over several subsequent cycles. b) SEM images of four subsequent cycles, showing the lateral growth at the termini of the seeds. c) Average length distribution of the fibers after each cycle (obtained by measuring the length of 50 fibers in SEM images in (b)). d) Emission spectra recorded during the first cycle. e) Development of the emission at λ_{max} in four subsequent cycles.

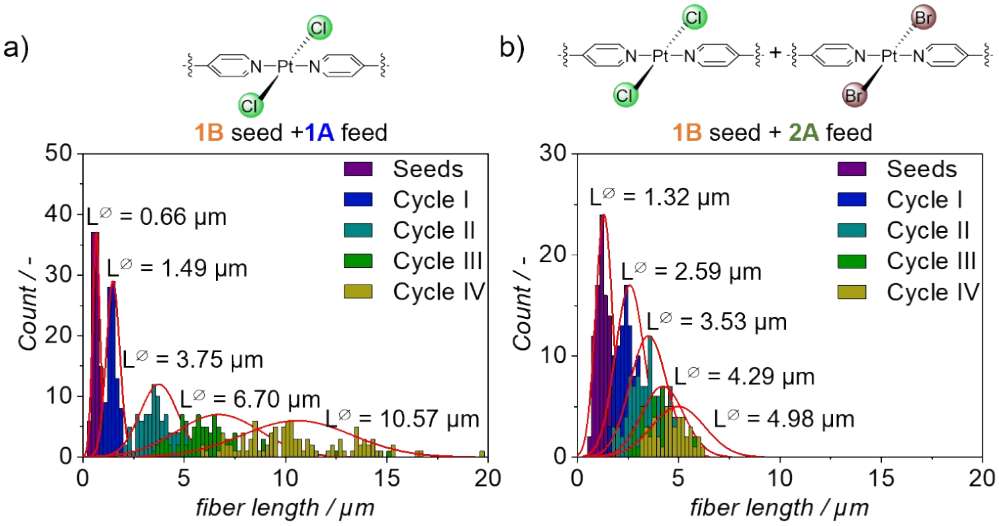

Figure S16. Comparison of the average length distribution of the fibers after each cycle of LSP for pristine **1B** (a) and addition of **2A** to seeds of **1B**, inducing growth of **2B** at its termini. The size distributions were obtained by measuring the length of 100 (a) or 50 (b) fibers in SEM images of the respective experiment.

The average length of the LSP of pristine **1B** (a) approximately doubles in each cycle, as it would be expected for a 1:1 dilution of the seeds in each cycle. In (b), in contrast, such a behavior is only observed in the first cycle, whereas the growth in length is continuously decreasing in the subsequent cycles.

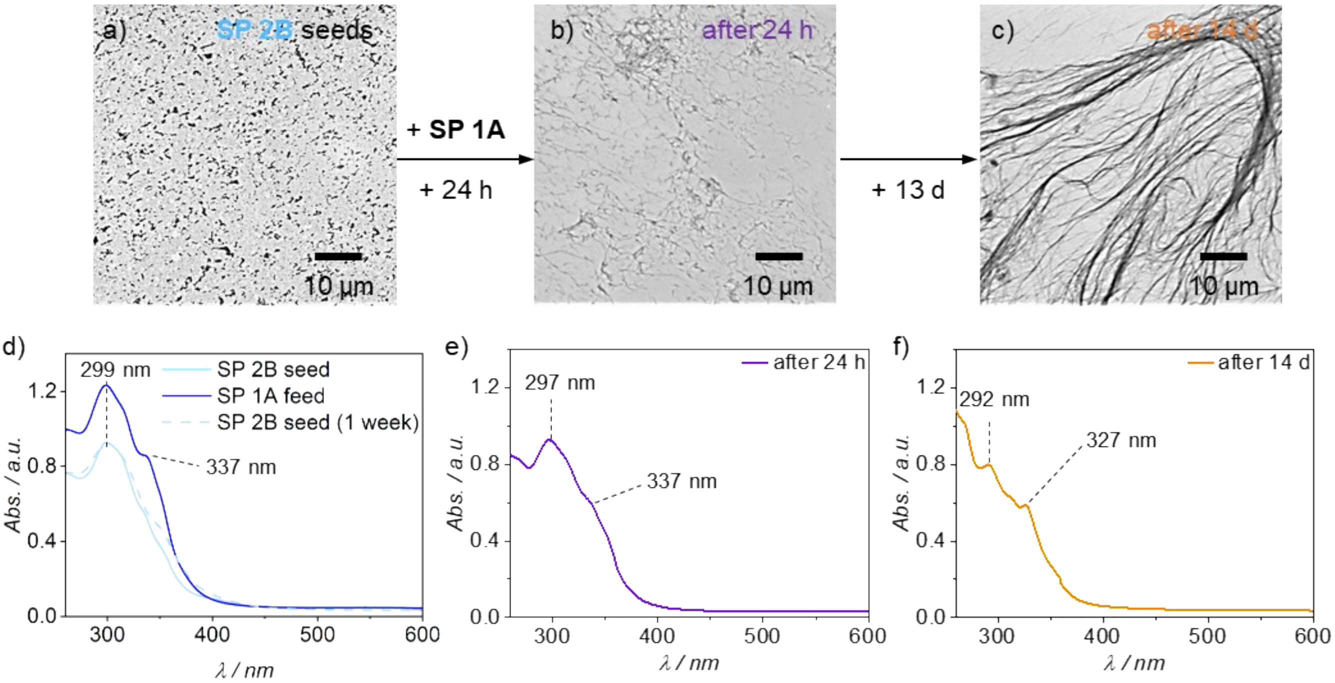

Figure S17. Hetero-seeding experiment with 1 eq **2B** seeds, inducing the growth of B-type SPs from a feedstock of 10 eq **1A** (experiment (2)). a-c) SEM images of **2B** seeds (a), the 1:10 mixture of **2B** seeds and **1A** after 24 h (b) and after 14 days (c). d-f) UV/vis spectra of the solutions, recorded prior to the SEM images. Time-dependent studies of 2B seeds after a week are added to Figure S17d (dotted cyan spectrum).

UV/Vis experiments revealed the high stability of the seeds of the kinetic product (**2B**) over time. In the SEM image recorded 24 h after addition of **1A** to the solution of **2B** seeds, thin SPs of **1A** are observed, whereas the smaller and diluted **2B** seeds cannot be distinguished. The corresponding absorption spectrum (e) exhibits spectral features which are rather reminiscent of **1A**, albeit λ_{max} is slightly blue-shifted. Hence, the great majority of the added 10 eq **1A** remains present as such and has not been converted to **1B**. However, after ageing the solution for 14 days, the spectral features clearly correspond to **1B**, which agrees with the SEM images showing elongated, thicker SP fibers.

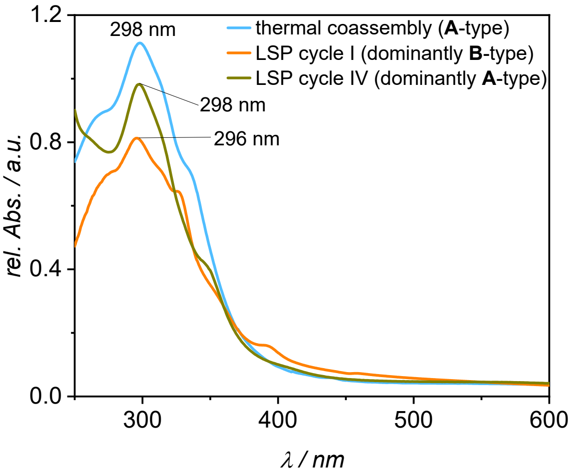

Figure S18: Comparison of the UV/Vis absorption spectra of thermally controlled- and seed-mediated co-assembly.

We have compared the UV/Vis spectra of the thermally controlled statistical co-assembly with the spectrum of the seed-mediated experiment (see figure S18). The spectral features of the thermally controlled statistical co-assembly are clearly of A-type copolymers with λ_{max} = 298 nm (cyan). The spectrum collected after completion of LSP-cycle I (orange) is clearly different, with the absorption maximum shifted to lower wavelengths as a result of the B-type nature of the block-copolymers in this cycle. In the following cycles, the further growth of the **2B**-segments is hampered by the accumulation of steric bulk of **2** and thus the solution is continuously diluted by larger amounts of **2A** which do not transform to B-type SPs. This is perfectly reflected in the shift of λ_{max} to 298 nm in cycle IV (brown) and the overall close resemblance to the spectra of the statistical A-type copolymer from the thermally controlled co-assembly.

Experimental Section

Materials and Methods

General Procedures

All solvents were dried according to standard procedures. Reagents were used as purchased. All air-sensitive reactions were carried out under argon or nitrogen atmosphere.

For all spectroscopic measurements, spectroscopic grade solvents were used.

Colum Chromatography

Preparative column chromatography was conducted in self-packed glass columns of different sizes with silica gel (*Merck Silica 60,* particle size 0.04 – 0.063 nm).

NMR measurements

^{1}H and ^{13}C NMR spectra were recorded on a *Bruker Avance II 300* (^{1}H: 300 MHz, ^{13}C: 75 MHz). and a *Bruker Avance II 400* (^{1}H: 400 MHz; ^{13}C: 101 MHz). Additional 1D ^{1}H spectra were recorded on an *Agilent DD2 500* (^{1}H: 500 MHz, ^{13}C: 126 MHz) and an *Agilent DD2 600* (^{1}H: 600 MHz, ^{13}C: 151 MHz) at a standard temperature of 298 K in deuterated solvents. The recorded spectra were referenced to the remaining resonance signals of the deuterated solvents. The coupling constant J of the measured spin multiplets is given in Hertz (Hz) and the chemical shift δ is given in reference to the chemical shift of trimethylsilane (0 ppm). Multiplicities for proton signals are abbreviated as *s, d, t, q, qui* and *m* for singlet, doublet, triplet, quadruplet, quintet and multiplet, respectively.

Mass spectrometry (MS)

MALDI mass spectra were recorded on a *Bruker Daltronics Ultraflex ToF/ToF* or a *Bruker Daltronics Autoflex Speed* with a *SmartBeamTM* NdYAF-Laser with a wavelength of 335 nm. The signals are described by their mass/charge ratio (*m/z*) in u.

UV/Vis absorption spectroscopy

UV/Vis absorption spectra were recorded on a *JASCO V-770* or a *JASCO V-750* with a spectral bandwidth of 1.0 nm and a scan rate of 1000 nm min^{-1} or on an *Agilent Cary 4000* with a spectral bandwidth of 2 nm at a scan rate of 600 nm min^{-1}. Glass cuvettes with an optical length of 1 cm, 1 mm and 0.1 mm and 0.01 mm were used. All measurements were conducted in commercially available solvents of spectroscopic grade.

Emission spectroscopy

Fluorescence emission and excitation spectra were recorded on a *JASCO Spectrofluorometer FP-8500* with an excitation and emission bandwidth of 5.0 nm at a scan rate of 1000 nm min^{-1}in quartz cuvettes with an optical length of 1 cm.

FTIR spectroscopy

All measurements were carried out using a *JASCO-FT-IR-6800*. Measurements in solution were performed using a CaF_2 transmission cell with a path length of 0.1 mm. Measurements in the solid state (thin films) were performed using a *JASCO ATR Pro-One* single reflection ATR accessory.

Scanning Electron Microscopy (SEM)

SEM images were recorded on a *Thermo Fisher Scientific Phenom ProX* Desktop SEM. The individual images were recorded with an acceleration voltage between 5 to 15 kV. A backscattered-electron detector (BSD) or a secondary-electron detector (SED) were used. All samples were prepared by drop-casting the sample onto Si wafer surfaces which were then dried under ambient conditions. Length analysis was conducted using the external program ImageJ.

Gel permeation chromatography (GPC)

Gel permeation chromatography was performed on a *Shimadzu prominence* GPC system equipped with a *Japan Analytical Industry Co., Ltd. JAIGEL-2HR* (20 mm I.D. x 600 mm) with $CHCl_3$ as eluent. The solvent flow was set to be 4 mL/min. Detection was carried out via a *Shimadzu prominence SPD-M20A* diode array detector (DAD).

Synthesis and Characterization

The pyridine-based oligo(phenylene-ethynylene) (OPE) ligand **L** with a bisamide-appended peripheral solubilizing moiety and chlorido complex **1** were synthesized according to a previously published protocols (Scheme S1).[2,3] Complex **2** was synthesized according to a standard complexation protocol using the ligand and bis(benzonitrile)dibromoplatinum(II) in chloroform at 70 °C.

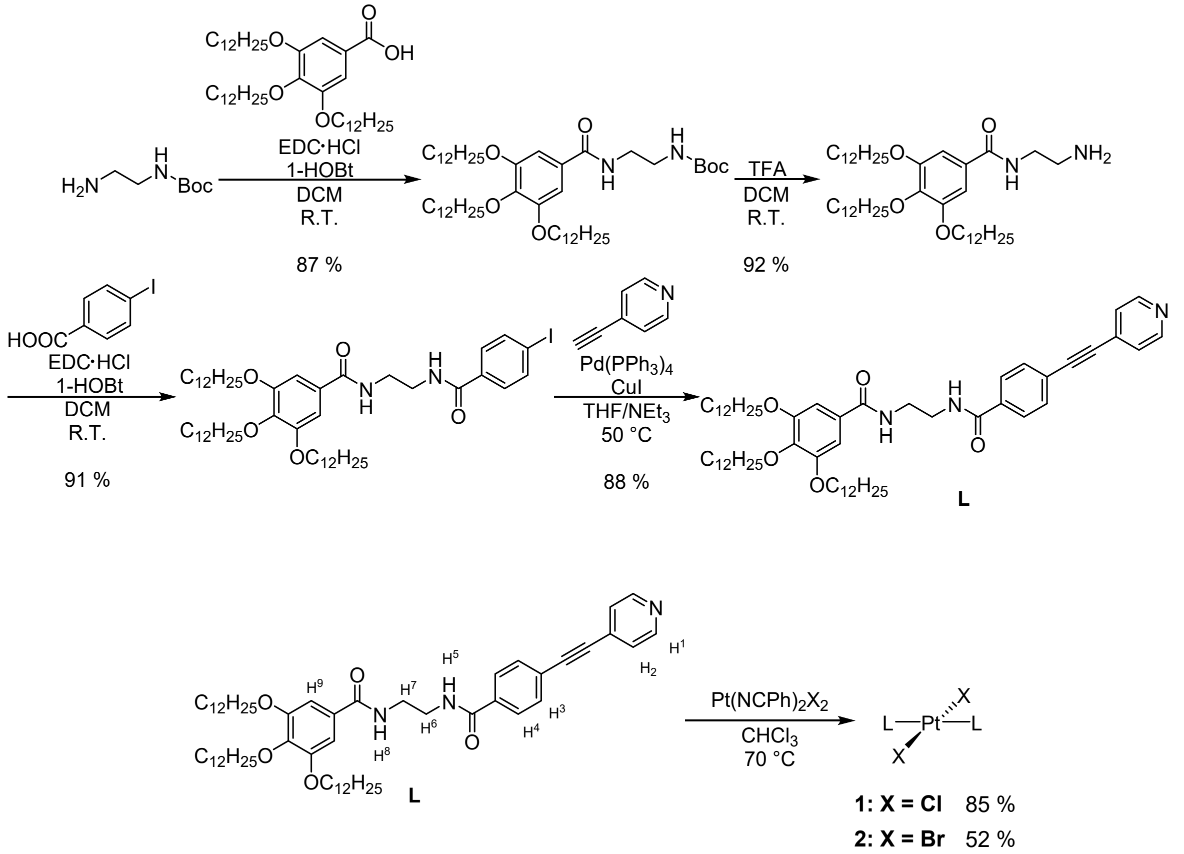

Scheme S1. Synthesis of ligand **L** and complexes **1** (Cl) and **2** (Br).

Complex 2

3,4,5-tris(dodecyloxy)-N-(2-(4-(pyridin-4-ylethynyl)benzamido)ethyl)benzamide **L** (20.0 mg; 21.7 µmol; 2.0 eq.) and bis(benzonitrile)dibromoplatinum(II) $Pt(NCPh)_2Br_2$ (6.1 mg; 10.8 µmol; 1.0 eq.) were placed in a Schleck tube and 2 mL of chloroform were added. The reaction mixture was stirred at 70 °C for three days. Subsequently, the reaction solution was filtered through a 0.2 µm PTFE syringe filter and was directly subjected to purification by means of gel permeation chromatography (eluent $CHCl_3$). After evaporation of the solvent *in vacuo*, the product was obtained as a yellow-orange solid (12.5 mg, 5.7 µmol, 51.6 %).

^{1}H NMR ($CDCl_3$, 600 MHz) δ(ppm) = 8.91 (m, 4H, H^1), 7.85 (m, 4H, H^4), 7.60 (m, 4H, H^3), 7.47 (t, 2H, NH^5), 7.33 (m, 4H, H^2), 7.00 (m, 6H, H^9 + NH^8), 4.00 (m, 12H, OCH_2), 3.71 (m, 8H, N-CH_2-CH_2-N), 1.80 (qui, 8H, $C^2H_2{}^a$), 1.73 (qui, 4H, $C^2H_2{}^b$), 1.46 (m, 12H, C^3H_2), 1.28 (m, 96H, C^4H_2-$C^{11}H_2$), 0.87 (t, *J* = 7.0 Hz, 18H, $C^{12}H_3$).

^{13}C NMR ($CDCl_3$, 126 MHz) δ (ppm) = 169.20, 167.51, 154.51, 154.04, 153.29, 141.48, 134.97, 132.43, 128.74, 127.45, 127.16, 124.62, 105.75, 87.38, 77.41, 77.16, 76.91, 73.68, 69.45, 41.73, 40.93, 32.09, 32.08, 30.47, 29.90, 29.89, 29.88, 29.86, 29.84, 29.82, 29.82, 29.80, 29.73, 29.56, 29.54, 29.52, 29.52, 26.26, 26.23, 22.84, 14.27.

HR-MS (MALDI-TOF, DCTB): calculated for $C_{135}H_{200}N_8O_{10}BrPt^+$ $[M+DCTB-Br]^+$: 2370.4247,
found: 2370.4164

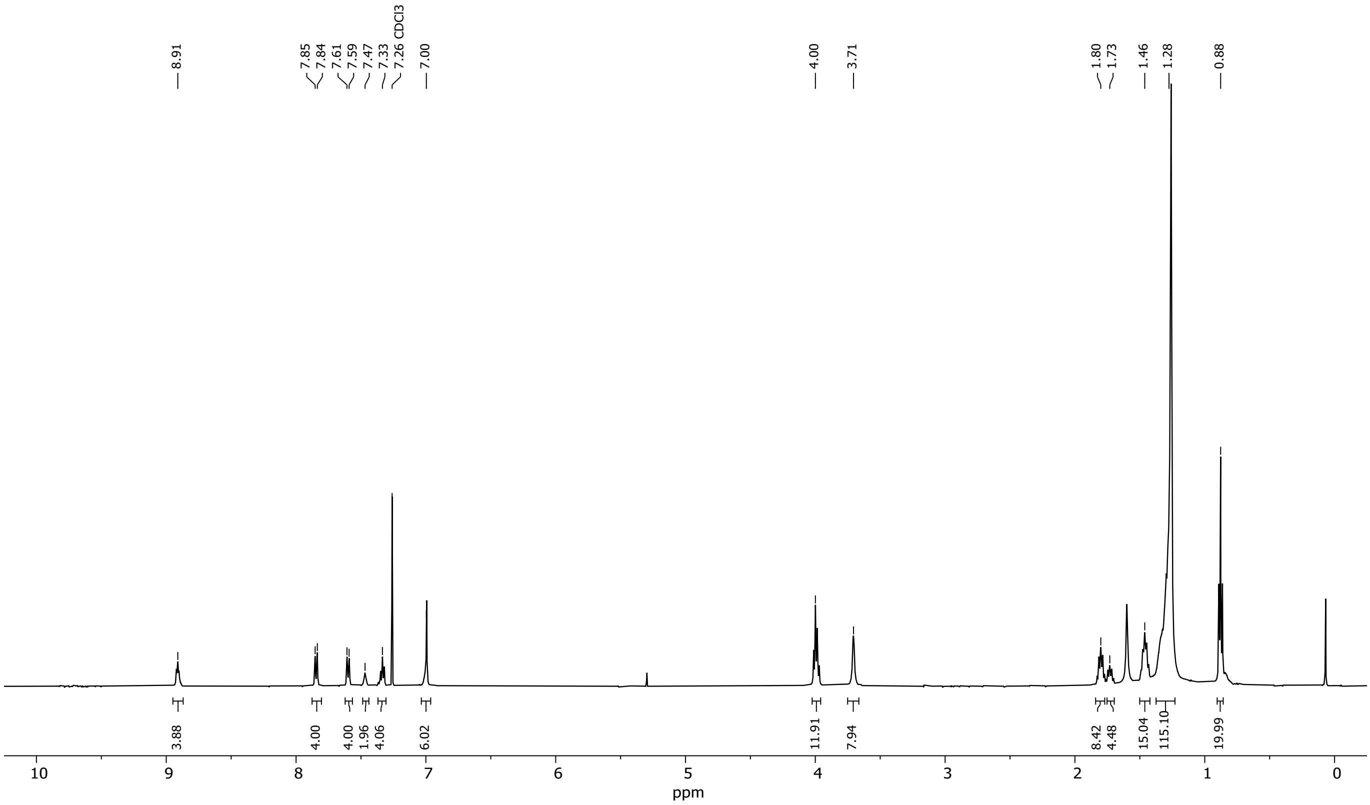

Figure S18. ^1H NMR ($CDCl_3$, 500 MHz) spectrum of bromido complex **2**.

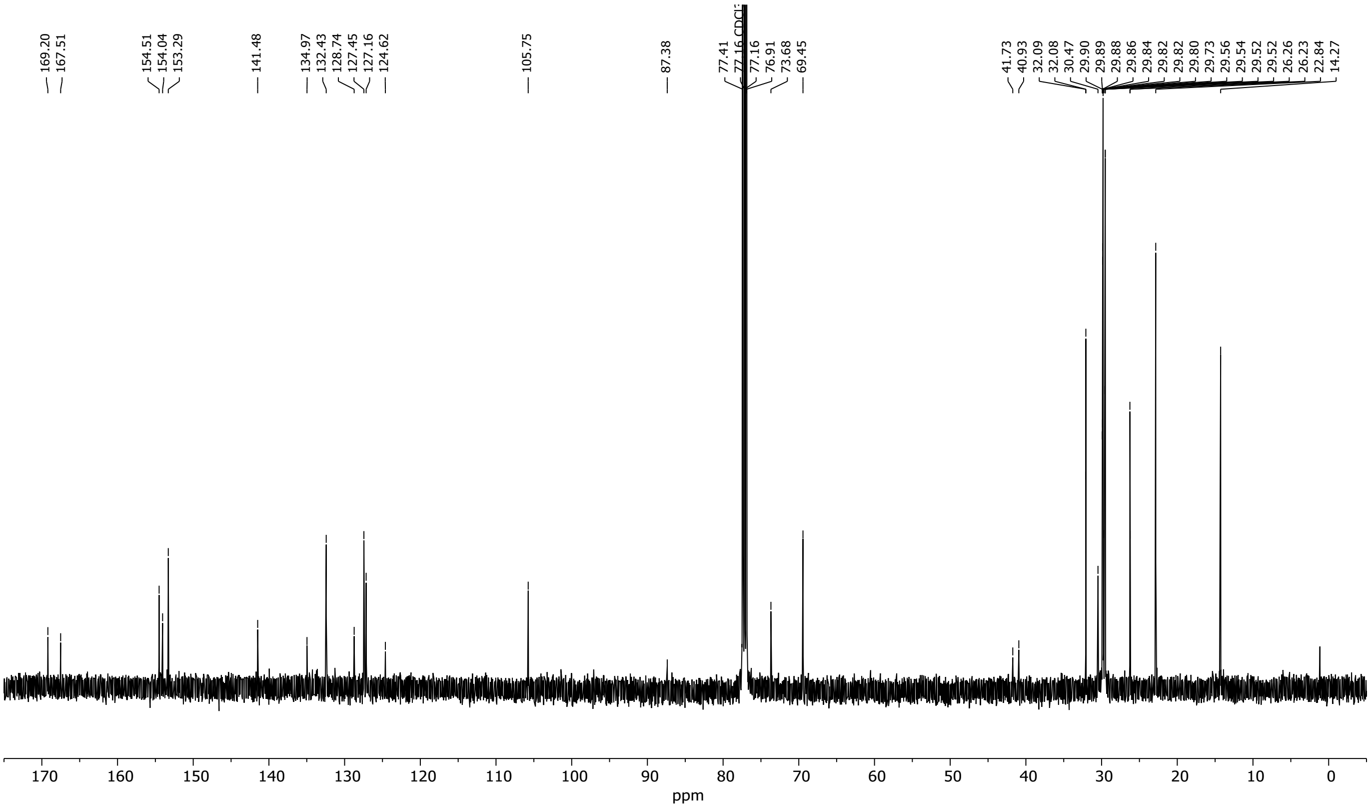

Figure S19. ^{13}C NMR ($CDCl_3$, 126 MHz) spectrum of bromido complex **2**.

References

1 J. Matern, N. Bäumer and G. Fernández, *J. Am. Chem. Soc.*, 2021, **143**, 7164.

2 J. Matern, I. Maisuls, C. A. Strassert and G. Fernandez, *Angew. Chem. Int. Ed.*, 2022, DOI: 10.1002/anie.202208436.

3 J. Matern, Z. Fernandez, N. Bäumer and G. Fernandez, *Angew. Chem. Int. Ed.*, 2022, e202203783.

Author Contributions

G.F. and J.M. conceived the project. J. M. performed most of the experiments and wrote the manuscript draft. Z. F. performed some spectroscopic studies, helped analyse the data. G.F. supervised the project and revised the manuscript, data and images. All authors were involved in the finalization of the manuscript.